Available online at www.sciencedirect.com
ScienceDirect
Trans. Nonferrous Met. Soc. China 32(2022) 3650−3662
Transactions of Nonferrous Metals Society of China
www.tnmsc.cn

Micromorphology and texture of niobium coating electrodeposited in NaCl−KCl−CsCl molten salt system

Shuang-peng HU, Shu-xin BAI, Li-an ZHU, Yi-cong YE, Zhen WANG, Shun LI, Yu TANG

College of Aerospace Science and Engineering, National University of Defense Technology, Changsha 410073, China

Received 30 August 2021; accepted 12 January 2022

Abstract: A low-toxicity and environment-friendly NaCl−KCl−CsCl−K_2NbF_7 system was used to prepare Nb coatings on Mo substrates. The effects of temperature, current density and electrodeposition time on the micromorphologies and textures of the electrodeposited Nb coatings were studied. The results showed that Nb coatings obtained at 30−70 mA/cm^2 in the temperature range of 700−750 °C were continuous and compact, with a hardness range of 2.16−2.45 GPa. As the columnar crystals grew with time, the preferential growth orientations of the Nb coatings changed from ⟨200⟩ to ⟨211⟩ and then became disordered. With increasing polarization, the morphologies of the Nb coatings changed from hexagonal star-like surface to conical or pyramid-like surface.

Key words: niobium coating; chloride molten salt; electrodeposition; micromorphology; texture

1 Introduction

Refractory metal niobium (Nb), with high melting point (2468 °C), relatively low density (8.57 g/cm^3), superior high-temperature strength, high thermal conductivity, small thermal neutron capture cross section, high superconducting critical temperature (9.2 K), good corrosion resistance and excellent biocompatibility, is usually used to fabricate critical components working in extreme conditions, such as superconductors, chemical reaction tanks, biological implants, rocket engine combustion chambers, reactor heat exchangers and nuclear reactors [1−4].

Nb coating should be characterized to enable commercial use in the most efficient manner because of its high cost and low content. The current preparation methods of Nb coatings mainly include thermal spraying (TS), physical vapor deposition (PVD), chemical vapor deposition (CVD) and electrodeposition (ED) in molten salt. TS, which has the advantages of low cost and high efficiency, is suitable for preparation of thick coatings that do not require high density and surface smoothness [5,6]. The Nb coatings prepared by PVD are smooth and dense. However, high cost and low deposition efficiency of PVD make it only suitable for preparing nano-scale thin films [7,8]. CVD, with moderate deposition rate and low device complexity, has been used to fabricate the Nb transition flange of iridium/rhenium combustion chambers [9,10]. But high processing temperatures (~1300 °C) and poor coating uniformity on complex-shaped substrates limit its widespread use. Although the electrolyte is toxic, ED, with high efficiency and deposition rate, is suitable for preparing uniform and dense Nb coatings on complex-shaped components at a constant rate ruled by the Faraday's law. So, it is one of the most promising methods to realize the large-scale industrial production of Nb coatings in the future [11,12].

Fluoride, chloride and fluorochloride are three common supporting electrolyte systems in the studies of ED Nb. MELLORS and SENDEROFF [13]

Corresponding author: Li-an ZHU, Tel: +86-15874139477, E-mail: mr_zla@163.com
DOI: 10.1016/S1003-6326(22)66046-1

prepared a continuous and dense Nb coating in a LiF−NaF−KF system. The prepared Nb coating, whose maximum thickness could reach 6.35 mm, with a typical columnar crystal structure, had a density over 99.8% of the theoretical density. However, fluoride, known to be highly toxic and polluting, often remains on the surface of the Nb coatings and is not easy to remove [14]. KUZNETSOV et al [15] successfully prepared a continuous, dense and smooth Nb coating in a NaCl−KCl−NaF system. But the fluoride content was still high from the perspective of environmental protection and health. Although the fluoride-free NaCl−KCl system is environmentally friendly and easy to clean, the polarization of chloride ions is relatively weak, resulting in poor stability of Nb complexes and thus poor compactness and adhesion of the prepared Nb coatings [13]. KOLOSOV and SHEVYREV [16] obtained a uniform and dense Nb coating on the rotor of a gryogenic gyroscope in a NaCl−KCl system with heavy addition of fluoride active salt to improve the stability of the Nb complexes. As the second coordination sphere cation, the counter- polarization action of Cs ions is relatively weak among the common cations, which can enhance the stability of the Nb complexes [17]. Therefore, the addition of CsCl in binary chloride system is supposed to both reduce the toxicity of the molten salt and at the same time ensure the stability of the Nb complexes, which is essential for preparing continuous and dense Nb coatings with good adhesion. However, as far as we know, there is little research on this kind of system so far. In order to further increase the stability of the molten salt mixture, K_2NbF_7 was selected as the active salt, due to its low vapor pressure, high stability and weak hygroscopicity [13].

In this work, we prepared Nb coatings on Mo substrates using a low-toxicity and environment-friendly NaCl−KCl−CsCl−K_2NbF_7 molten salt system. The effects of temperature, current density and electrodeposition time on the micromorphology and texture of ED Nb coatings were studied, laying a theoretical and technical foundation for the green production of high-quality Nb coatings.

2 Experimental

2.1 Experimental apparatus and pretreatments

Figure 1 shows the schematic diagram of apparatus for electrodeposition of Nb coatings in molten salt. The electrodes and crucible were placed in a closed cavity, where the electro-deposition was carried out under the protection of high-purity argon (99.999%). The temperature of the molten salt was monitored by a thermocouple with a molybdenum protection tube. A Mo plate (30 mm × 15 mm × 1 mm) and a Nb crucible were used as the cathode and anode, respectively. Before electrodeposition, the Mo substrates were polished with metallographic sandpapers, ultrasonically cleaned with ethanol for 5 min and dried in an oven at 120 °C; the Nb crucible was polished with a metallographic sandpaper, chemically cleaned with mixed acids of 35 vol.% HF and 10 vol.% HNO_3 for 1 min, ultrasonically cleaned with ethanol for 5 min and dried in an oven at 120 °C.

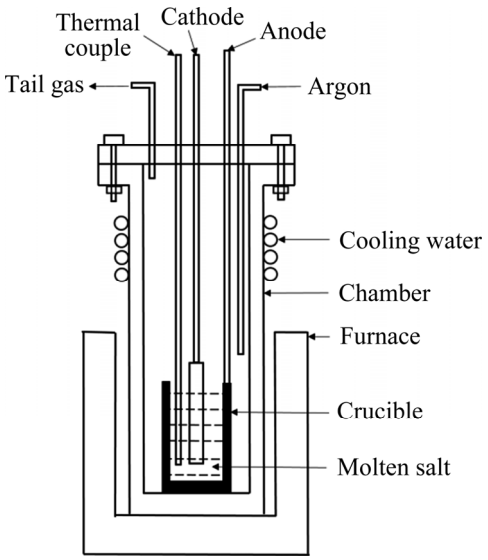

Fig. 1 Schematic diagram of apparatus for electro-deposition of Nb coatings in molten salt

Supporting electrolyte mixture (17.6wt.%NaCl−22.4wt.%KCl−60wt.%CsCl) was dried in an oven at 200 °C for 8 h, and then put into the cavity and heated to 750 °C in Ar atmosphere until melted. The chlorine was passed into the melts to remove impurities before the replacement of Ar to remove residual chlorine. The active salt K_2NbF_7, dried in a vacuum oven at 120 °C and 100 Pa for 8 h, was added into the above-mentioned purified supporting electrolyte until the Nb ion concentration reached 2.4 wt.%. All chemicals used in this study were of analytical grade.

2.2 Electrodeposition

The electrodeposition processing parameters of Nb coatings are shown in Table 1. Samples (1−5), (3, 6−10) and (3, 11−14) are for temperature (T), cathode current density (J), and electrodeposition time (t) rests, respectively.

Table 1 Electrodeposition processing parameters

Sample No.	T/°C	J/(mA·cm^{-2})	t/min
1	600	30	60
2	650	30	60
3	700	30	60
4	750	30	60
5	800	30	60
6	700	10	180
7	700	50	36
8	700	70	25.7
9	700	90	20
10	700	150	12
11	700	30	1
12	700	30	5
13	700	30	15
14	700	30	300

2.3 Characterization

The surface and fracture morphologies of the Nb coatings were observed by a MIRA3 LMH scanning electron microscope (SEM). The element compositions were detected by an Oxford X-MAX20 energy dispersive spectrometer (EDS). The phase compositions and preferred growth directions of the Nb coatings were measured by a Rigaku Ultima IV X-ray diffractometer (XRD) with a Cu K_α source, with a scanning rate of 10 (°)/min in the scanning range (2θ) of 10°−90°. Coating roughness was measured by a Zygo Newviewer 7100 optical profiler. Coating hardness was measured by an HMAS-C1000SZD hardness tester.

3 Results and discussion

3.1 Effect of temperature

Figure 2 shows the surface morphologies of Nb coatings prepared at different temperatures. As the temperature was below 650 °C, there were spherical-like and flower-like nodules distributed on the continuous and compact Nb coatings. According to EDS analyses (Fig. 3), the spherical-like nodules composed of pyramid-like grains were Nb, while the flower-like nodules contained ~41 at.% O element. With increasing temperature,

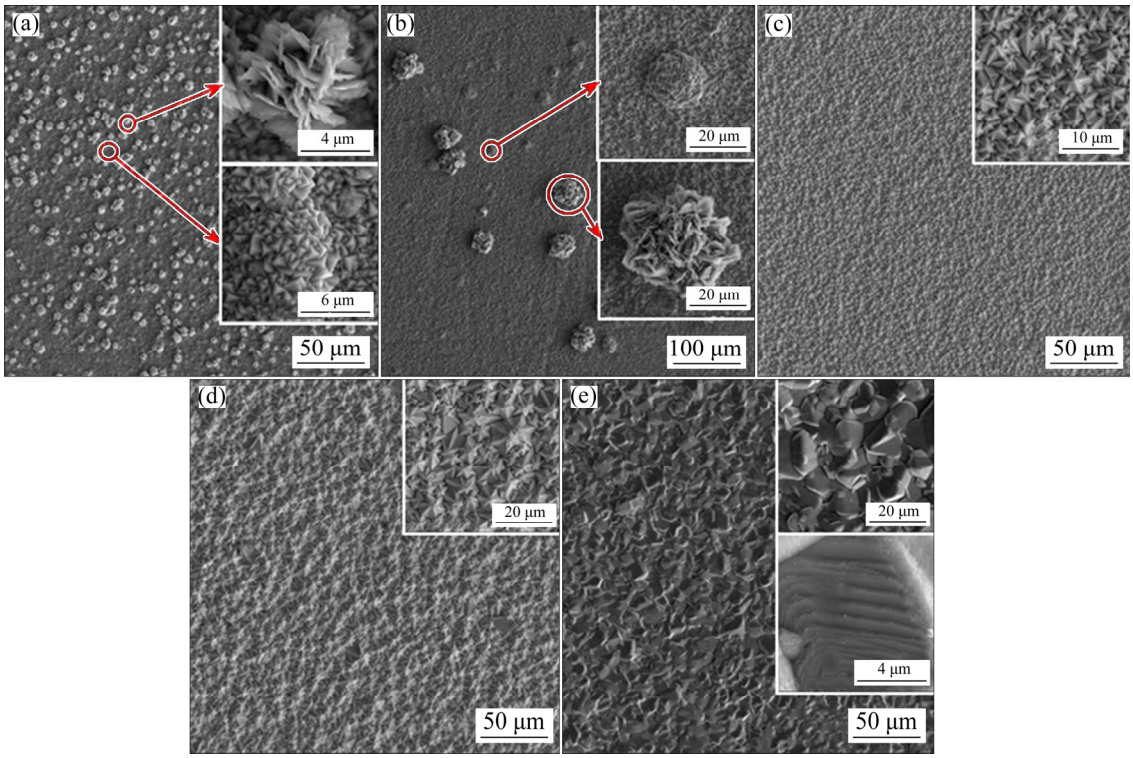

Fig. 2 SEM images of surface morphologies of Nb coatings prepared at different temperatures: (a) 600 °C; (b) 650 °C; (c) 700 °C; (d) 750 °C; (e) 800 °C

the nodules disappeared. The surface morphologies of the Nb coatings changed from pyramid to hexagonal star and then shell, with obvious grain coarsening. The morphology details of an individual shell (see inset in Fig. 2(e)) show that there are plenty of steps on the grain surface, which is probably related to a layered electrocrystalline growth mechanism. It is reported that when the temperature is lower than 650 °C, Nb^{2+} tends to exist stably in the form of oxides [18−21], thus resulting in the formation of flower-like nodules on the Nb coatings deposited at low temperatures. The formation of Nb^{2+} not only reduces the current efficiency, but also decreases the effective Nb ion concentration that can be reduced to the Nb coating, which further leads to the concentration polarization and thus the formation of spherical-like nodules.

As depicted in Fig. 4, all the ED Nb coatings are composed of a fine equiaxed crystal nucleation layer close to the substrate and a columnar crystal continuous growth layer. There are two competing processes, i.e., nucleation and growth, during the electrodeposition. In the early stage of electro-

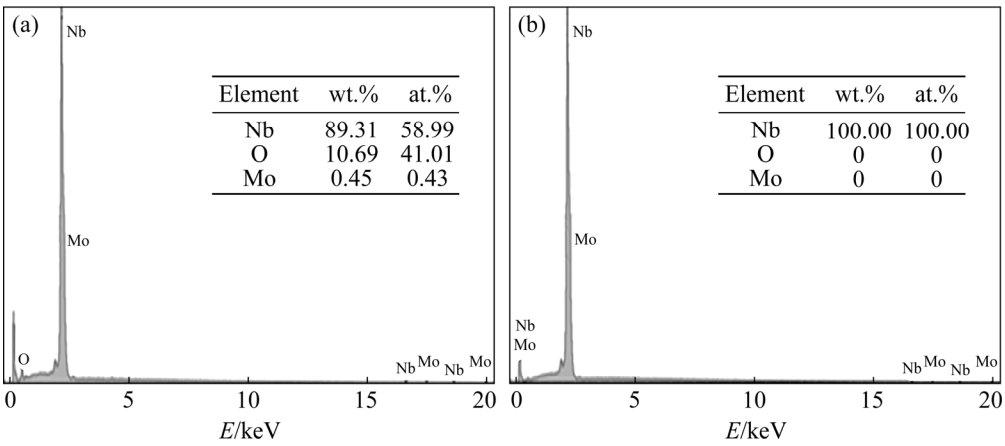

Fig. 3 EDS analysis results of flower-like grains (a) and pyramid-like nodules (b)

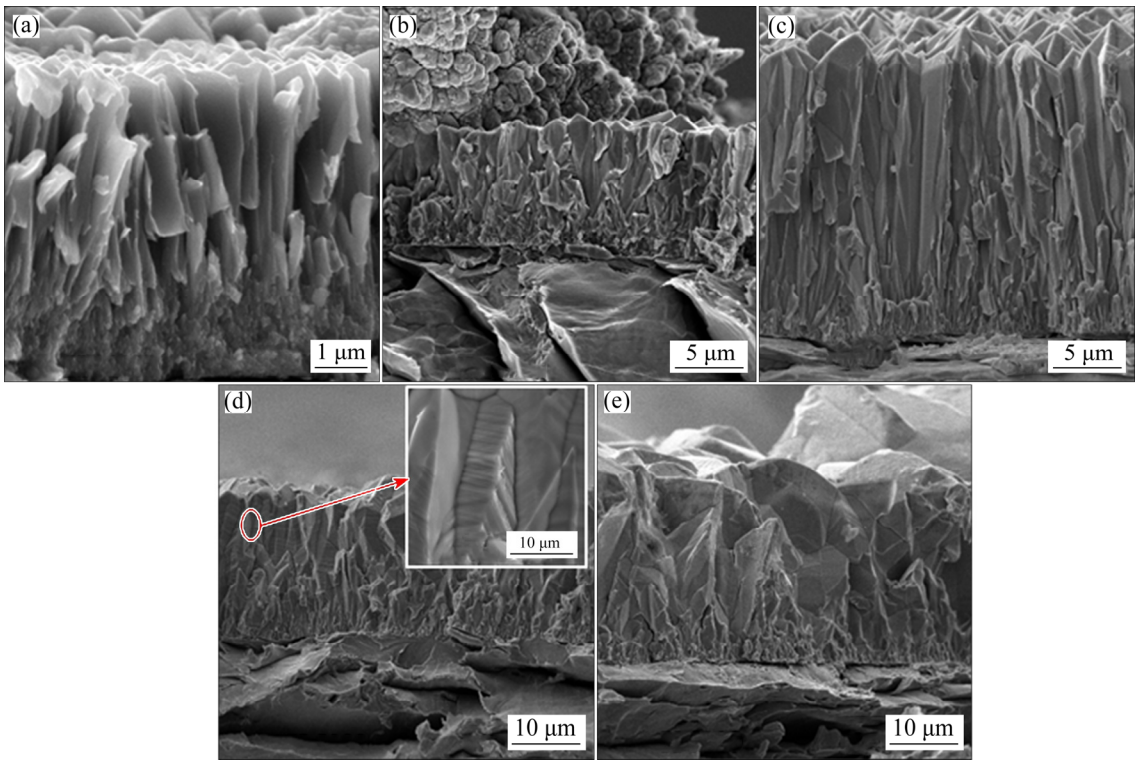

Fig. 4 SEM images of cross-sectional fracture morphologies of Nb coatings prepared at different temperatures: (a) 600 °C; (b) 650 °C; (c) 700 °C; (d) 750 °C; (e) 800 °C

deposition, the nucleation rate is commonly greater, forming a thin equiaxed nucleation layer. As the crystal grains grow, a tip discharge phenomenon occurs, the crystal growth rate increases and thus the crystals continue to grow to form a columnar continuous growth layer [22]. With increasing temperature, the diameter of the columnar crystals increases significantly. The cathodic reaction rate and ion diffusion rate increase with increasing temperature, which reduces the cathodic reaction overpotential and ion diffusion overpotential, resulting in a decrease in the nucleation rate and an increase in the growth rate [23,24]. The thicknesses of the Nb coatings obtained at 600 and 650 °C are 6.0 and 8.7 μm, respectively, which are much lower than that of the Nb coating obtained at other temperatures (~24.0 μm). When the temperature was below 650 °C the obviously subnormal thicknesses of the Nb coatings are caused by the formation of the nodules, which reduces the cathode current efficiency. The cathode current efficiency is an index reflecting the coating deposition efficiency under a certain deposition condition, which could be calculated according to Eq. (1):

$$\eta_e = m_{mea}/m_{cal} \times 100\% = \frac{JtSM}{ze_0 m_{cal}} \times 100\% \quad (1)$$

where m_{mea} is the measured mass of the Nb coating (sample mass gain), m_{cal} is the theoretical mass of Nb coating under an experimental condition, J is the cathode current density, t is the deposition time, S is the surface area of the cathode, M is the relative atomic mass of Nb, z is the valence state of Nb ion in molten salt (+5), and e_0 is the elementary electric charge.

The nodules fell off during ultrasonic cleaning, with the result that the current efficiencies of Nb coatings deposited at 600 and 650 °C are calculated to be 28% and 35%, respectively. As temperature is above 700 °C, the current efficiencies of the Nb coatings are close to 100%, with superior coating surface qualities and similar thicknesses. The surface roughness R_q (root mean square deviation) of the nodule-free Nb coatings is (2.17±0.06), (2.74±0.12) and (2.57±0.06) μm, respectively, with increasing temperature from 700, 750 and 800 °C. The hardnesses of the coatings deposited at 700, 750 and 800 °C, which were thick enough to perform a microhardness test, are (2.23±0.07), (2.43±0.10) and (2.16±0.07) GPa, respectively. The differences between these data are within the measurement error range, indicating that the correlation between temperature and coating hardness is weak.

As shown in Fig. 5, when the temperature was lower than 650 °C, Mo peaks could be found in the XRD patterns, indicating that the X-ray could penetrate the thin Nb coatings of at least 9 μm. It could be noticed that there were quite weak peaks

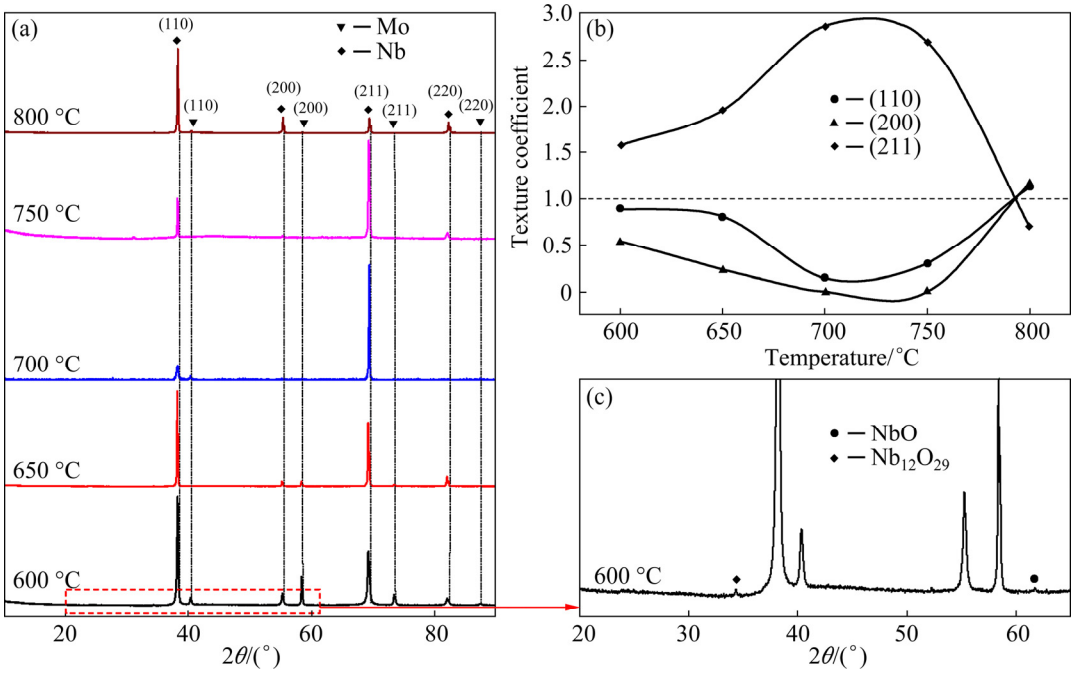

Fig. 5 XRD patterns of Nb coatings prepared at different temperatures (a, c) and texture coefficient as function of temperature (b)

of Nb oxides (NbO and $Nb_{12}O_{29}$) in the partial enlarged XRD pattern of the Nb coating deposited at 600 °C, confirming the stable existence of Nb oxides at low deposition temperatures. It is noticed that the relative intensities of the diffraction peaks of crystal planes changed with increasing temperature, indicating that the preferred orientation of Nb coating is temperature dependent. Texture coefficient (TC), which could quantitatively describe the preferential growth of each crystal plane in the Nb coating, is defined as the ratio of the relative diffraction intensity of a certain crystal plane to the average value of the diffraction intensity of each crystal plane, which can be calculated according to Eq. (2) [19]:

$$\mathrm{TC}_{(hkl)}=\frac{I_{(hkl)}/I'_{(hkl)}}{1/N\left[\sum I_{(hkl)}/I'_{(hkl)}\right]} \tag{2}$$

where $\mathrm{TC}_{(hkl)}$ is the texture coefficient of (*hkl*) crystal plane, $I_{(hkl)}$ and $I'_{(hkl)}$ represent the diffraction intensities of the (*hkl*) crystal planes of the Nb coating and the standard Nb powder, respectively, and N is the number of diffraction peaks. For polycrystalline powder samples, the texture coefficient of each crystal plane should be close to 1. On the contrary, if the texture coefficient of a certain crystal plane of the sample is greater than 1, it indicates that the crystal plane has a preferential growth orientation.

From a thermodynamic point of view, a coating has energy items such as surface energy and strain energy, exhibiting the preferential growth orientation at the lowest energy [25,26]. ZHANG et al [27] calculated the surface energy of each crystal plane of the BCC structure metal and found that $E_{(110)}<E_{(211)}<E_{(100)}$. If only the surface energy is considered, the crystal plane with the smallest surface energy should be the preferred growth plane in the coating [28], resulting in a preferential growth orientation of ⟨110⟩ [29]. However, due to the presence of strain energy and interface energy, the coating has nucleation textures [30,31] and growth textures [30,32]. From Fig. 4 and Fig. 5(b), it can be seen that when the temperature is lower than 800 °C, the coating has obvious columnar crystals with a preferential growth orientation of ⟨211⟩, in line with Pangarov model [31]. When the temperature increases to 800 °C, Nb grains of different orientations can nucleate and grow evenly due to the significantly decreased activation energies [33,34], resulting in columnar crystals coarsening and disordered growth orientation.

3.2 Effect of current density

Figure 6 shows the surface morphologies of the Nb coatings prepared at different current

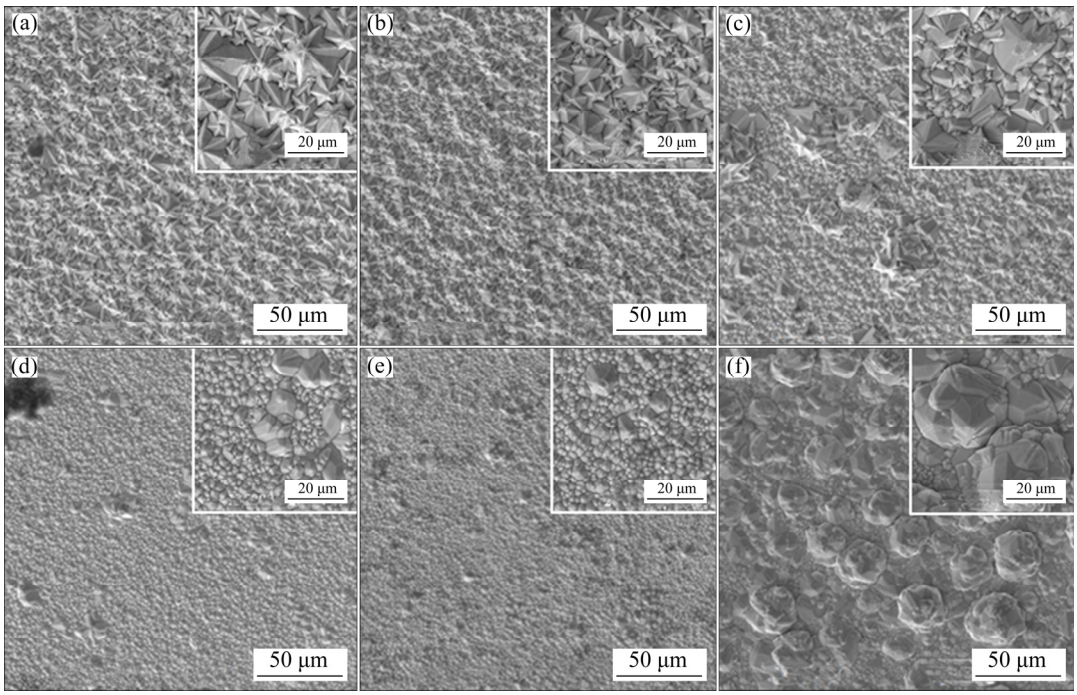

Fig. 6 SEM images of surface morphologies of Nb coatings prepared at different current densities: (a) 10 mA/cm^2; (b) 30 mA/cm^2; (c) 50 mA/cm^2; (d) 70 mA/cm^2; (e) 90 mA/cm^2; (f) 150 mA/cm^2

densities. The coating surfaces were composed of grains of different sizes. As the current density increased (except for 150 mA/cm^2), the proportion of large grains decreased. When the current density was below 30 mA/cm^2, the Nb coatings comprised hexagonal star shaped grain of varying sizes with a uniform surface morphology. When the current density increased to 50 mA/cm^2, the grain shape of the coating turned irregular with an uneven grain size distribution. When the current densities were 70 and 90 mA/cm^2, the grain morphologies changed to conical shapes, while the grain size difference was slightly reduced. When the current density reached 150 mA/cm^2, there were plenty of giant nodules of tens of microns on the coating surface, with a significant surface roughening.

The surface roughnesses and grain sizes of the Nb coatings prepared at current densities ranging from 10 to 90 mA/cm^2 are shown in Fig. 7 and Table 2, respectively. It can be seen that the roughness of the Nb coating increases firstly and then decreases with increasing current density, and the size of the crystal grains shows a downward trend. The current density changes the microstructure of the coating by essentially affecting the cathode overpotential [35]. The cathode overpotential increases as the current density increases, resulting in the decrease of the nucleation energy and critical nucleus radius. Therefore, the grain refinement becomes more significant with increasing current density.

When the current density was higher than 90 mA/cm^2, a ring could be found to grow at the three-phase interface of gas/molten salt(l)/solid cathode, i.e., around the electrode on the molten salt surface (see Fig. 8(a)). As the current density increased to 150 mA/cm^2, the area of the ring greatly increased, whose morphology and XRD pattern are shown in Figs. 8(b, c) and Fig. 9(a), respectively. The lower surface contacting with the melt was composed of big spherical particles, which comprised regular polygonal crystal grains, while the upper surface contacting the Ar atmosphere was smooth and uniform, composed of fine crystal grains. The XRD result indicates that the ring is Nb. It could be noticed that the Nb rings were only found under the deposition conditions of high current densities. Under such conditions, some light yellow deposits could be found on the water-cooling section of the deposition cavity, which were identified as $NaNbCl_6$ by XRD(see Fig. 9(b)). Considering the fact that the $NaNbCl_6$ is gaseous at 700 °C [36,37], it is inferred that the Nb ring forms due to the cathodic reduction reaction at the three-phase interface of $NaNbCl_6$(g)/molten salt(l)/cathode(s). Similar phenomenon has been observed in another molten system [38].

Table 2 Grain sizes of Nb coatings prepared at different current densities

Current density/ (mA·cm^{-2})	Large grain size/μm	Small grain size/μm	Average grain size/μm
10	13.2	5.9	6.6
30	10.3	4.4	5.9
50	16.3	3.9	5.5
70	7.9	2.2	2.4
90	5.9	2.8	2.0

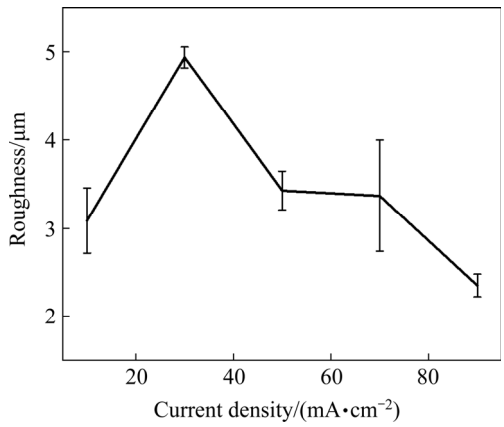

Fig. 7 Roughnesses of Nb coatings prepared at different current densities

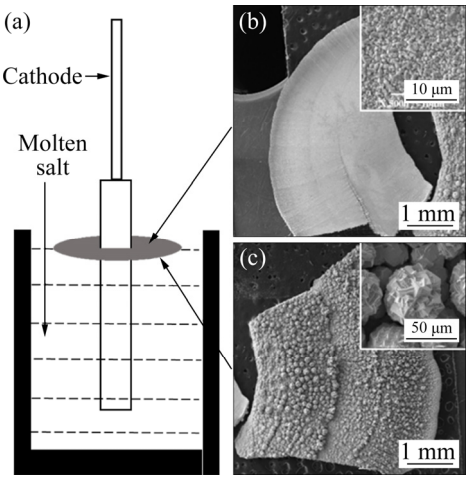

Fig. 8 Schematic diagram (a) and SEM images of lower surface (b) and upper surface (c) of ring growing at three-phase interface of gas/molten salt(l)/solid cathode and 150 mA/cm^2

As shown in Fig. 10, the ED Nb coatings exhibited classical double-layered structure, composed of a fine equiaxed crystal nucleation layer close to the substrate and a columnar crystal continuous growth layer. When the current density reached 150 mA/cm^2, the grains near the top of the coating exhibited abnormally grown spherical particles, similar to the inset of Fig. 8(c), rather than columnar crystals. We believe that the spherical morphology of the lower surface of the ring is formed by the electrodeposition at 150 mA/cm^2, considering the morphology similarity between Fig. 10(f) and Fig. 8(c). The hardnesses of the coatings are shown in Fig. 11. It can be found that the coating hardness exhibits upward trend with increasing current density. At the current density of 30−150 mA/cm^2, the coating hardness changes little, with an average value of ~2.27 GPa.

Figure 12 shows the XRD patterns and texture coefficients of each crystal plane of the Nb coatings prepared at different current densities. It can be seen that the preferential growth orientation keeps ⟨211⟩ unchanged as the current density increases. It shows that the preferred orientation of ED Nb

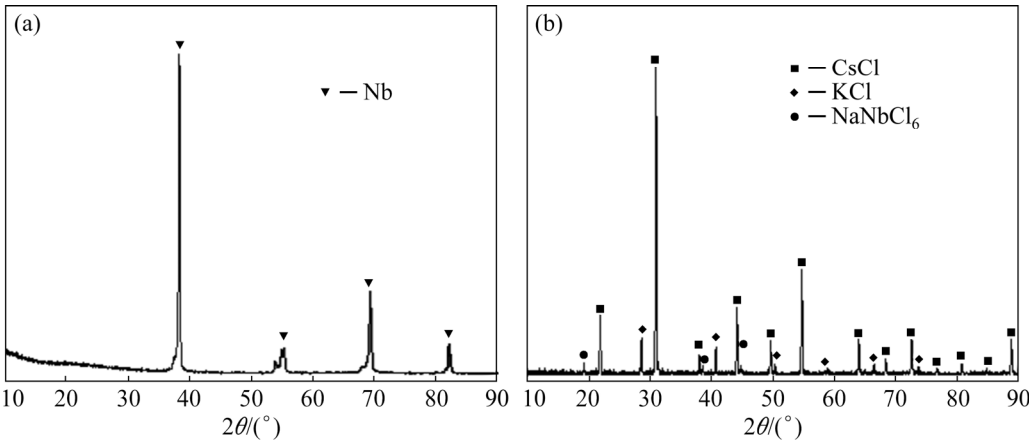

Fig. 9 XRD patterns of ring (a) and light yellow deposits (b)

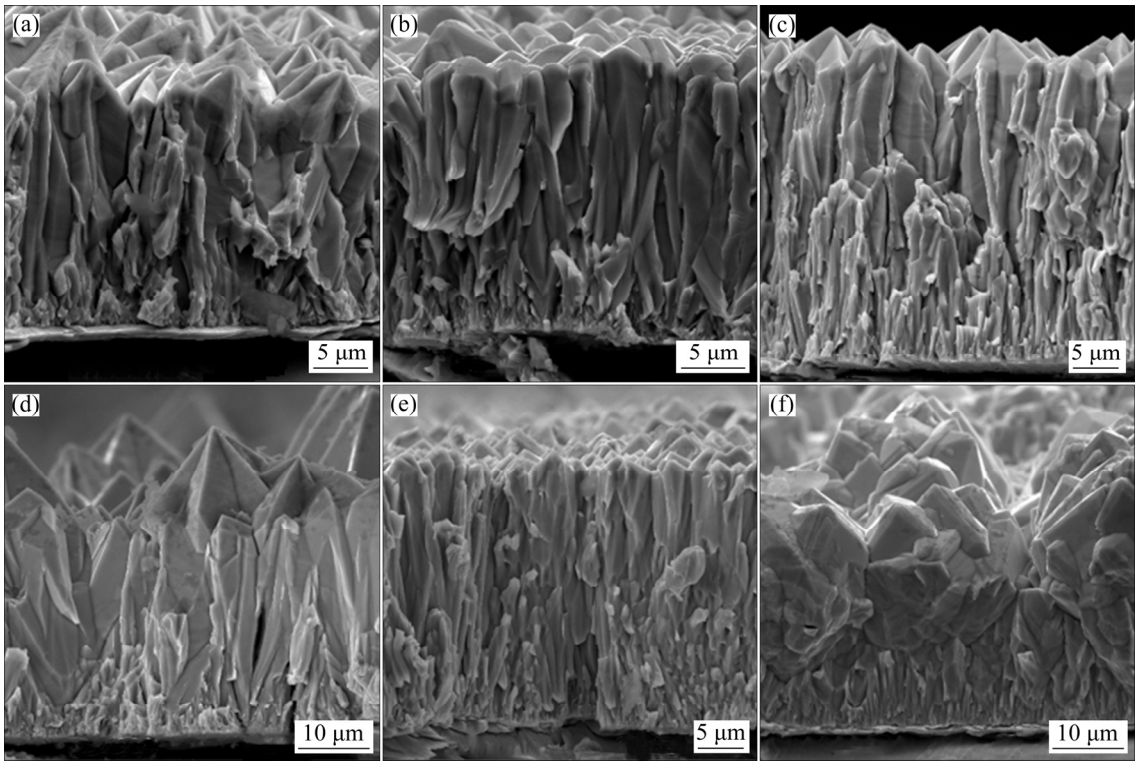

Fig. 10 SEM images of cross-sectional fracture morphologies of Nb coatings prepared at different current densities: (a) 10 mA/cm^2; (b) 30 mA/cm^2; (c) 50 mA/cm^2; (d) 70 mA/cm^2; (e) 90 mA/cm^2; (f) 150 mA/cm^2

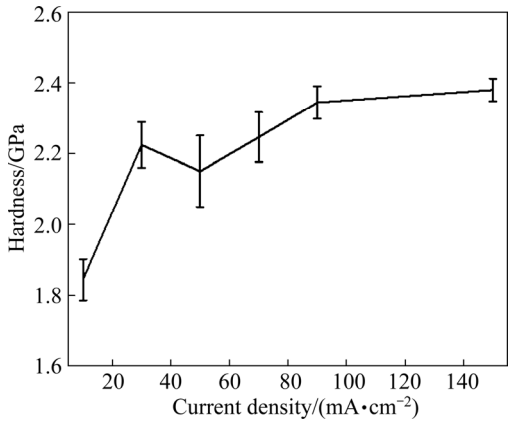

Fig. 11 Hardnesses of Nb coatings prepared at different current densities

coating has a small relationship with the current density within the current density range of this study.

3.3 Effect of electrodeposition time

Figures 13(a) and (b) show the surface morphologies of the as-received Mo substrate and the Mo substrate soaked in molten salt for 10 min, respectively. After 10 min soaking, discontinuous micron-level polyhedral-like crystal grains were uniformly distributed on the surface of the substrate. According to the EDS test (see Fig. 14), the crystal grains were Nb. Considering the fact that the Nb crucible was used as the active anode, the Nb reacts

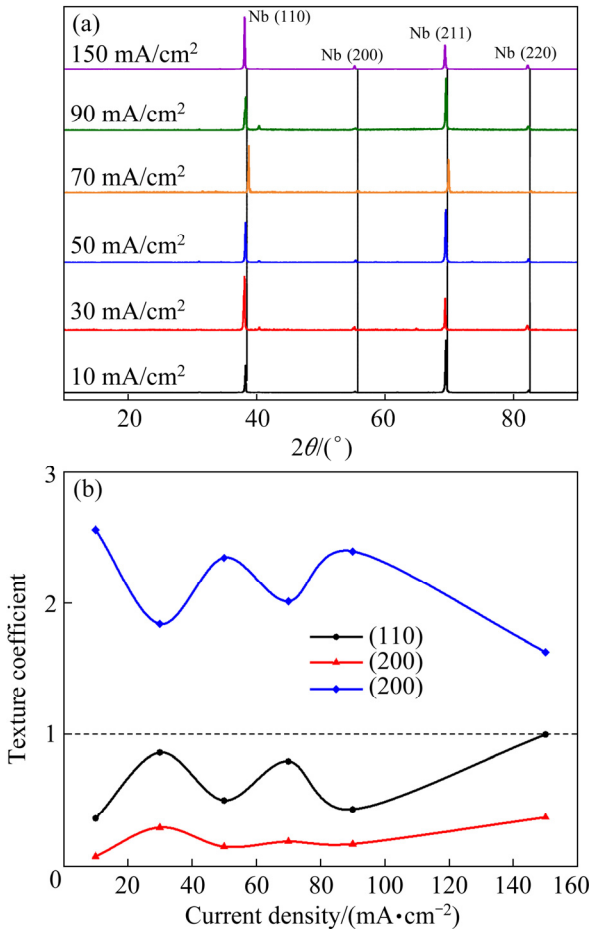

Fig. 12 XRD patterns of Nb coating prepared at different current densities (a) and texture coefficient as function of current density (b)

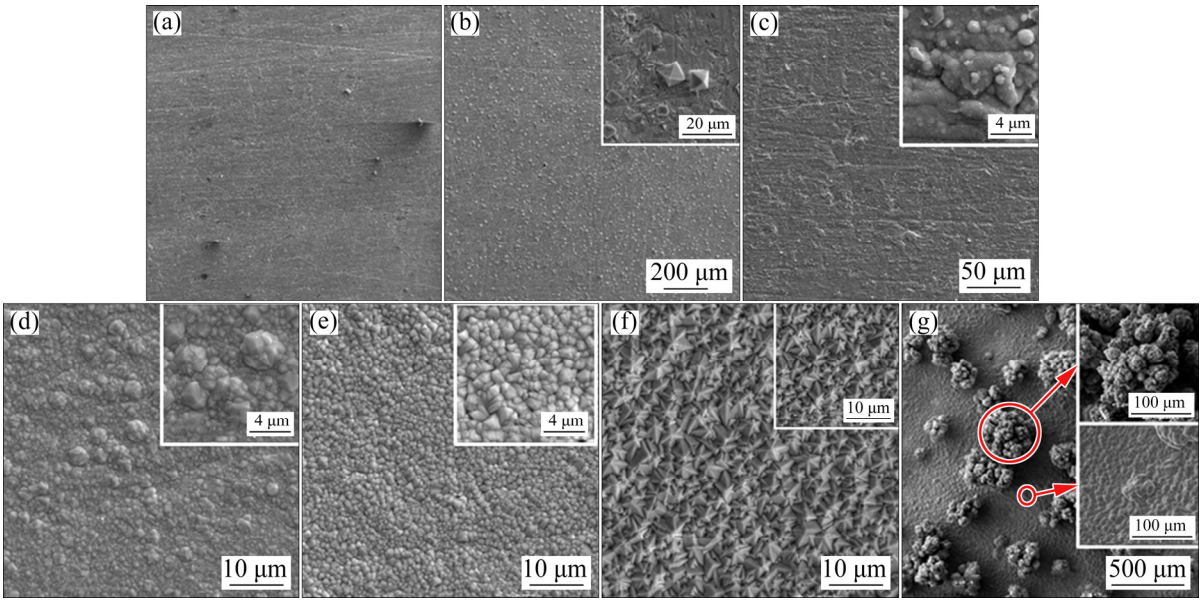

Fig. 13 SEM images showing surface morphologies of substrate (a, b) and coatings (c−g) under different conditions: (a) 0 min (i.e., substrate surface); (b) Soaked in molten salt for 10 min; (c) Electrodeposition for 1 min; (d) Electrodeposition for 5 min; (e) Electrodeposition for 15 min; (f) Electrodeposition for 60 min; (g) Electrodeposition for 300 min

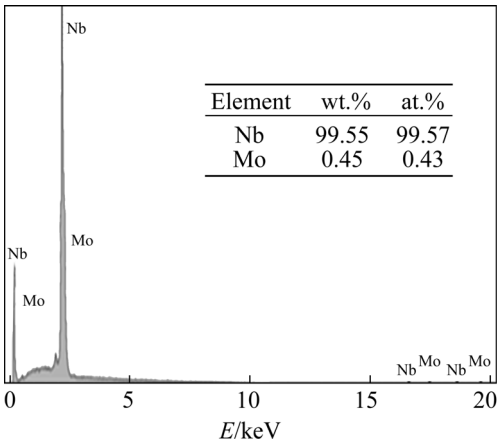

Fig. 14 EDS analysis results of polyhedral-like crystal grains

with the Nb^{5+} in the molten salt before electrodeposition [39,40]:

$$Nb+4Nb^{5+}\rightleftharpoons 5Nb^{4+} \quad (3)$$

The heat dissipation of the cathode matrix will produce a temperature gradient, which drives the disproportionation reaction of Nb^{4+} on the surface of the matrix [41], thereby forming Nb crystal grains on the surface of substrate. Figures 13(c−g) show the surface morphologies of the Nb coatings prepared at different deposition time. After electrodeposition for only 1 min, a continuous Nb coating composed of irregular small particles completely covered the substrate surface, with a few crevices and micropores in the coating. After 5 min, the Nb coating, comprising fine conical grains, became more uniform and continuous, with less crevices and micropores. After 15 min, the grain size of the coating increased and became more uniform. When the deposition time was extended to 60 min, the coating surface was composed of hexagonal star shaped grains of varying sizes. As the deposition time reached 300 min, huge protruding spherical Nb clusters started to form on the smooth and continuous coating composed of conical grains.

As shown in Fig. 15, the nucleation was completed only within 1 min deposition, and the thickness of the Nb coating was less than 1.00 μm. After that, the columnar structure of the coating gradually developed with increasing time. The thickness of the Nb coating increased proportionally with increasing deposition time, with grain coarsening and surface roughening.

Figure 16 exhibits the XRD patterns and the texture coefficients of Nb coatings prepared at different electrodeposition time. When the electrodeposition time was less than 15 min, obvious Mo

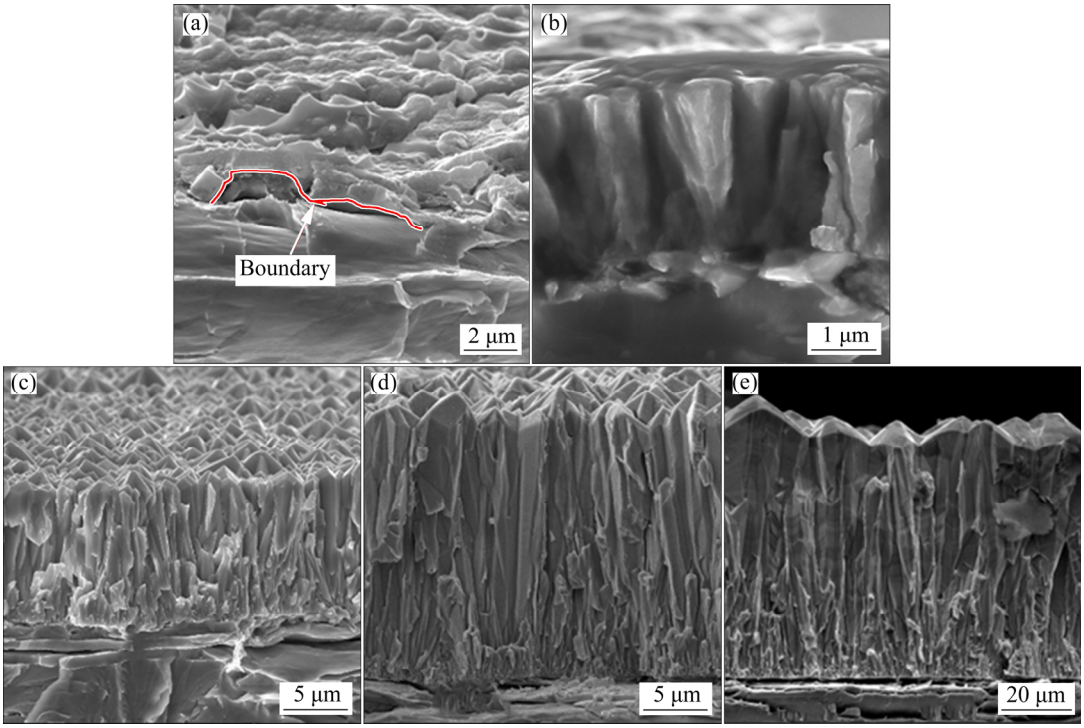

Fig. 15 SEM images showing cross-sectional fracture morphologies of Nb coatings prepared at different deposition time: (a) 1 min; (b) 5 min; (c) 15 min; (d) 60 min; (e) 300 min

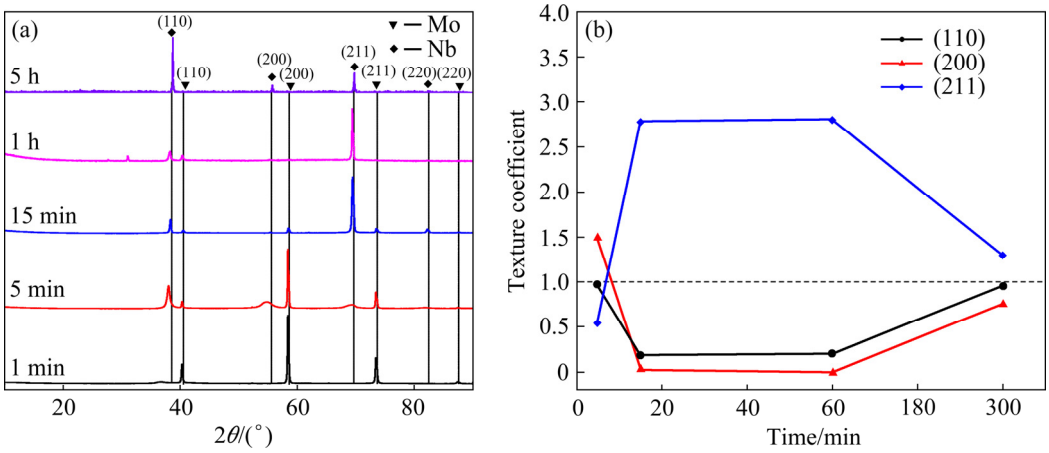

Fig. 16 XRD patterns (a) and texture coefficients (b) of Nb coatings prepared at different electrodeposition time

peaks could be found in the XRD patterns. The calculation shows that the texture coefficient in the Mo matrix (200) direction is 2.44, so it has the same preferred orientation in the ⟨200⟩ direction as the coating obtained at 5 min with a thickness of 2.97 μm. Considering the fact that Nb and Mo, both with BCC structure, have close lattice constants (Nb: 3.30 Å, Mo: 3.15 Å), epitaxial growth is prone to occur at the initial stage of coating deposition, thus the orientation of the formed thin film is generally the same as the texture of the substrate [30]. As the deposition time increases, the preferential growth orientation changed to ⟨211⟩ and finally disorder. From Figs. 5 and 12, the preferred orientation of ⟨211⟩ is a typical growth texture of ED Nb. The texture coefficient of (211) plane increases firstly, and then keeps constant and finally decreases sharply with increasing deposition time. It can be seen that the growth texture strengthens with thickening of the coating until the concentration polarization occurs as the active ions are depleted after long-term deposition. The formed powders are composed of randomly oriented spherical dendrites [42], thereby turning the preferred orientation into disorder.

4 Conclusions

(1) The morphologies and textures of Nb coatings electrodeposited on Mo substrates in a NaCl−KCl−CsCl melt containing 2.4 wt.% Nb were systematically studied at 10−150 mA/cm^2 in the temperature range from 600−800 °C.

(2) The cathode overpotential increases as the current density increases or the temperature decreases, resulting in the grain refinement of the Nb coatings. The roughness of the Nb coating increases firstly and then decreases with increasing current density, with a maximum value at 30 mA/cm^2. The coating hardness is roughly in the range of 2.16−2.45 GPa, showing a weak correlation with temperature and current density.

(3) All of the ED Nb coatings obtained at 10−90 mA/cm^2 and 600−750 °C were composed of a fine equiaxed crystal nucleation layer close to the substrate and a columnar crystal continuous growth layer. As the columnar crystals grew with time, the preferential growth orientations of the Nb coatings changed from ⟨200⟩ to ⟨211⟩ and then disordered. With decreasing polarization (i.e., decreasing current density or increasing temperature), the morphologies of the Nb coatings changed from conical or pyramid-like surface to hexagonal star-like surface.

(4) The optimal deposition process range for dense and smooth Nb coatings is as follows: temperature of 700−750 °C and current density of 30−70 mA/cm^2.

Acknowledgments

This work was supported by the Special Fund of Hunan Province for Innovative Province Building – Support Program for Young Talents of Hunan, China (No. 2020RC3034).

References

[1] REN Jun-shuai, ZHANG Ying-ming, GUO Xue-pen, XI En-ping, WANG Juan. Preparation of high purity niobium ingot for RF superconducting cavity [J]. Rare Metal

Materials and Engineering, 2019, 48(2): 688−692. (in Chinese)

[2] DENG Li-qin, XU Qian, LI Bing, ZHAI Yu-chun, HUANG Zhen-qi. Preparation of niobium by direct electrochemical reduction of solid Nb_2O_5 [J]. The Chinese Journal of Nonferrous Metals, 2005, 15(4): 541−545. (in Chinese)

[3] OLIVARES-NAVARRETE R, OLAYA J J, RAMÍREZ C, RODIL S E. Biocompatibility of niobium coatings [J]. Coatings, 2011, 1(1): 72−87.

[4] CAI Zhen-yang, SHEN Hong-tai, LIU Sai-nan, CHEN Yi-jie, PU Rong, CAO Qin-xuan, ZHANG Bei, XIAO Lai-rong, ZHAO Xiao-jun. Review and prospect of refractory metal alloys and high temperature oxidation resistance coatings [J]. The Chinese Journal of Nonferrous Metals, 2020, 30(9): 1991−2010. (in Chinese)

[5] BRANDOLT C S, NORONHA L C, HIDALGO G E N, TAKIMI A S, SCHROEDER R M, MALFATTI C F. Niobium coating applied by HVOF as protection against hydrogen embrittlement of API 5CT P110 steel [J]. Surface and Coatings Technology, 2017, 322: 10−18.

[6] NAEIMIAN H, MOFID M A. TLP bonding of Ti−6Al−4V to Al 2024 using thermal spray Babbitt alloy interlayer [J]. Transactions of Nonferrous Metals Society of China, 2020, 30(5): 1267−1276.

[7] PENG Ming-di, LU wei-er, XIA yang, WANG Tong, ZHAO Li-li, LI Nan. Study on preparation and properties of superconducting niobium films by pulsed laser deposition [J]. Materials Review, 2018, 32(S1): 105−109. (in Chinese)

[8] ZHANG Xiao-feng, NIU Shao-peng, DENG Zi-qian, LIU Min, LI Hong, DENG Chun-ming, DENG Chang-guang, ZHOU Ke-song. Preparation of Al_2O_3 nanowires on 7YSZ thermal barrier coatings against CMAS corrosion [J]. Transactions of Nonferrous Metals Society of China, 2019, 29(11): 2362−2370.

[9] TUFFIAS R, BROCKMEYER J, FORTINI A, WILLIAMS B, DUFFY A, KAPLAN R. Engineering issues of iridium/ rhenium rocket engines revisited [C]//The 35th AIAA/ ASME/SAE/ASEE Joint Propulsion Conference and Exhibit. Los Angeles: AIAA, 1999: 2752−2757.

[10] STECHMAN C, WOLL P, FULLER R, COLETTE A. A high performance liquid rocket engine for satellite main propulsion [C]//The 36th AIAA/ASME/SAE/ASEE Joint Propulsion Conference and Exhibit. Huntsville: AIAA, 2000: 3161−3169.

[11] MARENKOVA E A, KUZNETSOV S A. Complex formation and micropassivation at electrodeposition of niobium coatings in alkali chloride−fluoride melts with different cationic composition [J]. ECS Transactions, 2013, 50(11): 263−275.

[12] DUBROVSKIY A, OKUNEV M, MAKAROVA O, KUZNETSOV S. Superconducting niobium coatings deposited on spherical substrates in molten salts [J]. Coatings, 2018, 8(6): 213.

[13] MELLORS G W, SENDEROFF S. Electrodeposition of coherent deposits of refractory metals: I. Niobium [J]. Journal of the Electrochemical society, 1965, 112(3): 266.

[14] KUZNETSOV S A. Electrochemistry of refractory metals in molten salts: Application for the creation of new and functional materials [J]. Pure and Applied Chemistry, 2009, 81(8): 1423−1439.

[15] KUZNETSOV S A, MARENKOVA E A, KALINNIKOV V T. Micropassivation and complexation during electro-deposition of niobium coatings [J]. Doklady Chemistry, 2015, 463(1): 169−173.

[16] KOLOSOV V N, SHEVYREV A A. Deposition of superconducting Nb_3Sn and high-purity Nb coatings on the rotor of a cryogenic gyroscope [J]. Inorganic Materials, 2012, 48(2): 132−137.

[17] KUZNETSOV S A. Electrodeposition of niobium coatings on long conductors from a copper alloy [J]. Journal of the Electrochemical Society, 2019, 166(13): D694−D699.

[18] SENDEROFF S, MELLORS G W. The electrodeposition of coherent deposits of refractory metals: IV. The electrode reactions in the deposition of niobium [J]. Journal of the Electrochemical Society, 1966, 113(1): 66.

[19] PATIL P S, CHIGARE P S, SADALE S B, SETH T, AMALNERKAR D P, KAWAR R K. Thickness-dependent properties of sprayed iridium oxide thin films [J]. Materials Chemistry and Physics, 2003, 80(3): 667−675.

[20] BARHOUN A, BERGHOUTE Y, LANTELME F. Electrodeposition of niobium from fluoroniobate K_2NbF_7 solutions in fused NaCl−KCl [J]. Journal of Alloys and Compounds, 1992, 179(1/2): 241−252.

[21] PICARD G S, BOCAGE P. Niobium chemistry in molten LiCl+KCl eutectic [J]. ECS Proceedings Volumes, 1992, 16(1): 622−631.

[22] YOUSEFI E, IRANNEJAD A, SHARAFI S. Electrodeposition and characterization of nanocrystalline Fe−Ni−Cr alloy coatings synthesized via pulse current method [J]. Transactions of Nonferrous Metals Society of China, 2019, 29(12): 2591−2603.

[23] LI Xing-wu, RUAN Ying, WEI Bing-bo. Electrodeposition processing and mechanical properties of porous Cu [J]. The Chinese Journal of Nonferrous Metals, 2019, 29(3): 517−524. (in Chinese)

[24] HUANG Yong-le, BAI Shu-xin, ZHANG hong, YE Yi-cong. Growth mechanism and mechanical property of laminar iridium coating by electrodeposition [J]. International Journal of Refractory Metals and Hard Materials, 2015, 50: 204−209.

[25] WANG Yuan, SONG Zhong-xiao, XU Ke-wei. The surface mapping and crystal orientation of body-centered cubic thin metal tungsten films of different thickness [J]. Acta Physica Sinica, 2007, 56(12): 7248−7254.

[26] PELLEG J, ZEVIN L Z, LUNGO S, CROITORU N. Reactive-sputter-deposited TiN films on glass substrates [J]. Thin Solid Films, 1991, 197(1/2): 117−128.

[27] ZHANG Jian-min, WANG Dou-dou, XU Ke-wei. Calculation of the surface energy of bcc transition metals by using the second nearest–neighbor modified embedded atom method [J]. Applied Surface Science, 2006, 252(23): 8217−8222

[28] MOUROUX A, ZHANG S L, PETERSSON C S, PALMANS R, MAEX K, AHLGREN T, KEINONEN J. An experimental study of chemical vapour deposition of tungsten on Ti/TiN adhesion bilayers: mechanical properties [J]. Surface and Coatings Technology, 1998, 99(3): 274−280.

[29] THOMPSON C V. Secondary grain growth in thin films of

semiconductors: Theoretical aspects [J]. Journal of Applied Physics, 1985, 58(2): 763−772.
[30] KOLOSOV V N, SHEVYREV A A. Structure and texture of electrolytic superconducting coatings of high-purity niobium [J]. The Physics of Metals and Metallography, 2014, 115(8): 786−792.
[31] PANGAROV N A. Crystallite orientation in electro-deposition of metals [M]. Boston: Springer Publishers, 1976: 62.
[32] BUDEVSKI E, STAIKOV G, LORENZ W J. Electrocrystallization: nucleation and growth phenomena [J]. Electrochimica Acta, 2000, 45(15/16): 2559−2574.
[33] JAGTAP P, KUMAR P. Manipulating crystallographic texture of Sn coatings by optimization of electrodeposition process conditions to suppress growth of whiskers [J]. Journal of Electronic Materials, 2015, 44(4): 1206−1219.
[34] QIAN Jian-gang, LUAN Hai-jing, LI Peng-rui, LI Hai-ting. Preparation of iridium layer by electrodeposition in BMIC ionic liquid [J]. Rare Metal Materials and Engineering, 2013, 42(9): 1969−1972. (in Chinese)
[35] WANG Wen-chao, YANG Jian-guang, CHEN Bing, ZENG Wei-zhi. Simulation of tin membrane electrodeposition in chloride system [J]. The Chinese Journal of Nonferrous Metals, 2020, 30(1): 180−193. (in Chinese)
[36] LI Jun-li, YANG Dong-mei, ZENG Fan-wu, WANG Zhi-chang. Thermodynamic properties of $NbCl_5$−NaCl and $NbCl_5$−KCl binary systems by quenching experiments [J]. Transactions of Nonferrous Metals Society of China, 2006, 16(6): 1120−1124.
[37] SADOWAY D R, FLENGAS S N. The synthesis and properties of the hexachloroniobates and hexachloro-tantalates of Na, K, Rb, and Cs [J]. Canadian Journal of Chemistry, 1978, 56(15): 2013−2018.
[38] CHEN X, ZHAO H J, XIE H W, QU J K, DING X Y, GENG Y F, WANG D H, YIN H Y. Tuning the preferentially electrochemical growth of carbon at the "gaseous CO_2-liquid molten salt-solid electrode" three-phase interline [J]. Electrochimica Acta, 2019, 324: 134852.
[39] ALIMOVA Z A, POLYAKOV E G, POLYAKOVA L P, STANGRIT P T, KREMENETSKIJ V G. Interaction of niobium with chloride−fluoride niobium-containing melts [J]. Zhurnal Prikladnoj Khimii, 1990, 63(5): 992−999.
[40] POLYAKOV E G, POLYAKOVA L P, ELIZAROVA I R. Cathode processes in chloride−fluoride melts containing K_2NbF_7 [J]. Russian Journal of Electrochemistry, 1995, 31(5): 457−464.
[41] KOLOSOV V N, SHEVYREV A A. Structure, texture, and properties of superconductive electrolytic niobium coatings on nickel and copper substrates [J]. The Physics of Metals and Metallography, 2015, 116(5): 482−490.
[42] AVRAMOVIĆ L, IVANOVIĆ E R, MAKSIMOVIĆ V M, PAVLOVIĆ M M, VUKOVIĆ M, STEVANOVIĆ J S, NIKOLIĆ N D. Correlation between crystal structure and morphology of potentiostatically electrodeposited silver dendritic nanostructures [J]. Transactions of Nonferrous Metals Society of China, 2018, 28(9): 1903−1912.

NaCl−KCl−CsCl 熔盐体系电沉积铌涂层的微观形貌和织构

胡双鹏，白书欣，朱利安，叶益聪，王 震，李 顺，唐 宇

国防科技大学 空天科学学院，长沙 410073

摘 要：采用一种低毒、环保的 NaCl−KCl−CsCl−K_2NbF_7 体系在 Mo 基体上制备 Nb 涂层。研究温度、电流密度和沉积时间对电沉积 Nb 涂层微观形貌和织构的影响。结果表明，当温度为 700~750 ℃、电流密度为 30~70 mA/cm^2 时，可制备出连续致密的 Nb 涂层，其硬度为 2.16~2.45 GPa。随着柱状晶不断生长，Nb 涂层的择优取向按〈200〉→〈211〉→无序的顺序转变。随着极化程度的增大，Nb 涂层从六角星形表面变为锥形或金字塔形表面。

关键词：铌涂层；氯化物熔盐；电沉积；微观形貌；织构

(Edited by Wei-ping CHEN)